Quantifying the historic and future response of karst spring discharge to climate variability and change at a snow-influenced temperate catchment in central Europe

Xinyang Fan[1,2*], Nadine Goeppert[1], Nico Goldscheider[1]

[1]Institute of Applied Geosciences, Division of Hydrogeology, Karlsruhe Institute of Technology (KIT), 76131, Karlsruhe, Germany
[2]Department of Infrastructure Engineering & Melbourne Climate Futures Academy, University of Melbourne, 3053, Melbourne, Australia

**Correspondence to*: Xinyang Fan (xinyang.fan@partner.kit.edu)

Electronic supplementary material – Hydrogeology Journal

S1 Calibration of the observed discharge data

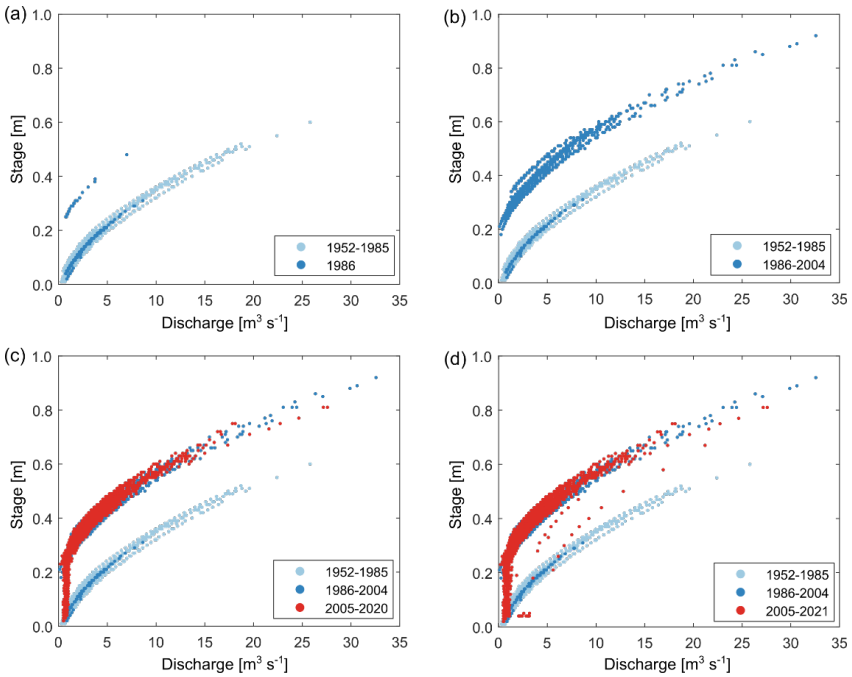

Fig. S1 The stage-discharge relationships at Blautopf in (a) 1952-1986, (b) 1952-2004, (c) 1952-2020, (d) 1952-2021.

Table S1 The second-degree polynomial regression of the stage (H) -discharge (Q) relationships at Blautopf. The regression is expressed as $Q = b_2 \times H^2 + b_1 \times H +$ intercept, and the performance is evaluated with R^2. The stage has a unit of m, and the discharge has a unit of $m^3\ s^{-1}$.

Year	Intercept	b_1	b_2	R^2
1952-1985	0.01	0.05	-0.002	0.95
1987-2004	0.22	0.05	-0.001	0.94
2005-2020	0.19	0.06	-0.002	0.72

S2 Climate data

S2.1 Parameter calibration for the Degree-Day Factor (DDF) method

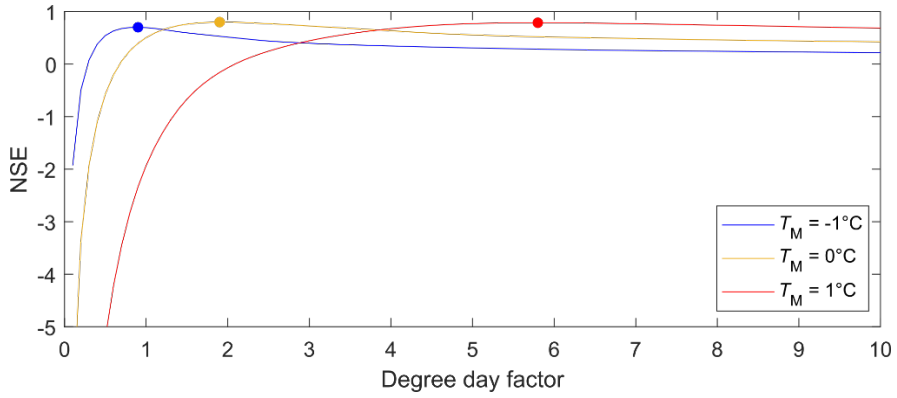

Fig. S2 The calibrated NSE with different combinations of the DDF factor and the T_M parameter in the DDF method. The NSE is used to evaluate the difference between the catchment snow storage (snow water equivalent) estimated with the DDF method and that observed at station 3402; an NSE equal to 1 means the best performance. The DDF factor is calibrated between 0.1-10 and the T_M is calibrated at -1, 0, and 1°C. The dot represents the NSE maximum obtained for each pair of the T_M and the DDF factor. The DDF = 1.9 and T_M = 0°C are identified as the best parameter set that gives the highest NSE (0.80) among all parameter sets.

S2.2 Extra-terrestrial radiation estimation with the FAO method (Allen et al. 1998)

$$R_e = \frac{24 \times 60}{\pi} G_{sc} d_r [\omega_s \sin(\varphi) \sin(\delta) + \cos(\varphi) \cos(\delta) \sin(\omega_s)] \quad (S1)$$

$$d_r = 1 + 0.033 \cos\left(\frac{2\pi}{365} J\right) \quad (S2)$$

$$\omega_s = \arccos[-\tan(\varphi) \tan(\delta)] \quad (S3)$$

$$\varphi = \frac{\pi}{180} \text{lat} \quad (S4)$$

$$\delta = 0.409 \sin\left(\frac{2\pi}{365} J - 1.39\right) \quad (S5)$$

where R_e is the extra-terrestrial radiation [MJ m^{-2} day^{-1}], G_{sc} is the solar constant equal to 0.082 MJ m^{-2} min^{-1}, d_r is the inverse relative Earth-Sun distance estimated with Eq. S2, ω_s is the sunset hour angle estimated with Eq. S3,

φ is the latitude [radians] of the weather station which is converted with Eq. S4 from the latitude [°], δ is the solar decimation [radians] estimated with Eq. S5, J is the Julian day between 1 and 365 or 366, lat is the latitude [°] of the weather station.

S2.3 The GCM-RCM members adopted for the three climate change scenarios

Table S2 The GCM-RCM members of each climate change scenario (Wunsch et al. 2022).

Climate scenario	GCM-RCM member
RCP 2.6	ICHEC-EC-EARTH_rcp26_r12i1p1_CLMcom-CCLM4-8-17_v1
	ICHEC-EC-EARTH_rcp26_r12i1p1_KNMI-RACMO22E_v1
	MIROC-MIROC5_rcp26_r1i1p1_CLMcom-CCLM4-8-17_v1
	MOHC-HadGEM2-ES_rcp26_r1i1p1_KNMI-RACMO22E_v2
	MPI-M-MPI-ESM-LR_rcp26_r2i1p1_MPI-CSC-REMO2009_v1
RCP 4.5	ICHEC-EC-EARTH_rcp45_r1i1p1_KNMI-RACMO22E_v1
	ICHEC-EC-EARTH_rcp45_r12i1p1_KNMI-RACMO22E_v1
	ICHEC-EC-EARTH_rcp45_r12i1p1_SMHI-RCA4_v1
	MOHC-HadGEM2-ES_rcp45_r1i1p1_CLMcom-CCLM4-8-17_v1
	MPI-M-MPI-ESM-LR_rcp45_r1i1p1_MPI-CSC-REMO2009_v1
	MPI-M-MPI-ESM-LR_rcp45_r2i1p1_MPI-CSC-REMO2009_v1
RCP 8.5	CCCma-CanESM2_rcp85_r1i1p1_CLMcom-CCLM4-8-17
	ICHEC-EC-EARTH_rcp85_r1i1p1_KNMI-RACMO22E
	MIROC-MIROC5_rcp85_r1i1p1_GERICS-REMO2015
	MOHC-HadGEM2-ES_rcp85_r1i1p1_CLMcom-CCLM4-8-17
	MPI-M-MPI-ESM-LR_rcp85_r1i1p1_UHOH-WRF361H
	MPI-M-MPI-ESM-LR_rcp85_r2i1p1_MPI-CSC-REMO2009_v1

S3 Statistical analysis of the discharge and climate

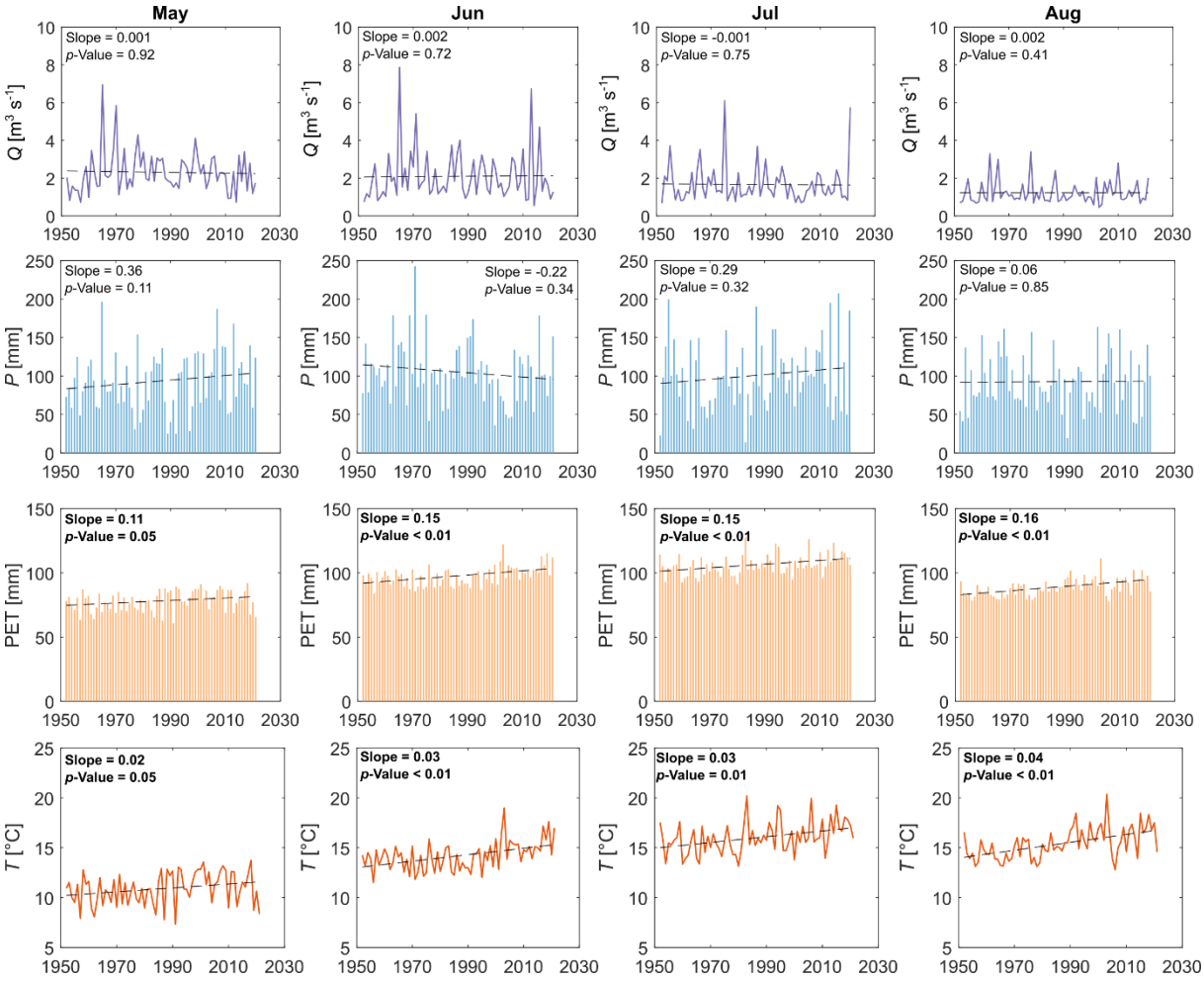

Fig. S3 Trends of the monthly mean discharge (*Q*), total precipitation (*P*), total potential evapotranspiration (PET), and mean temperature (*T*) in May, June, July, and August from 1952 to 2021. The dashed line represents the trend.

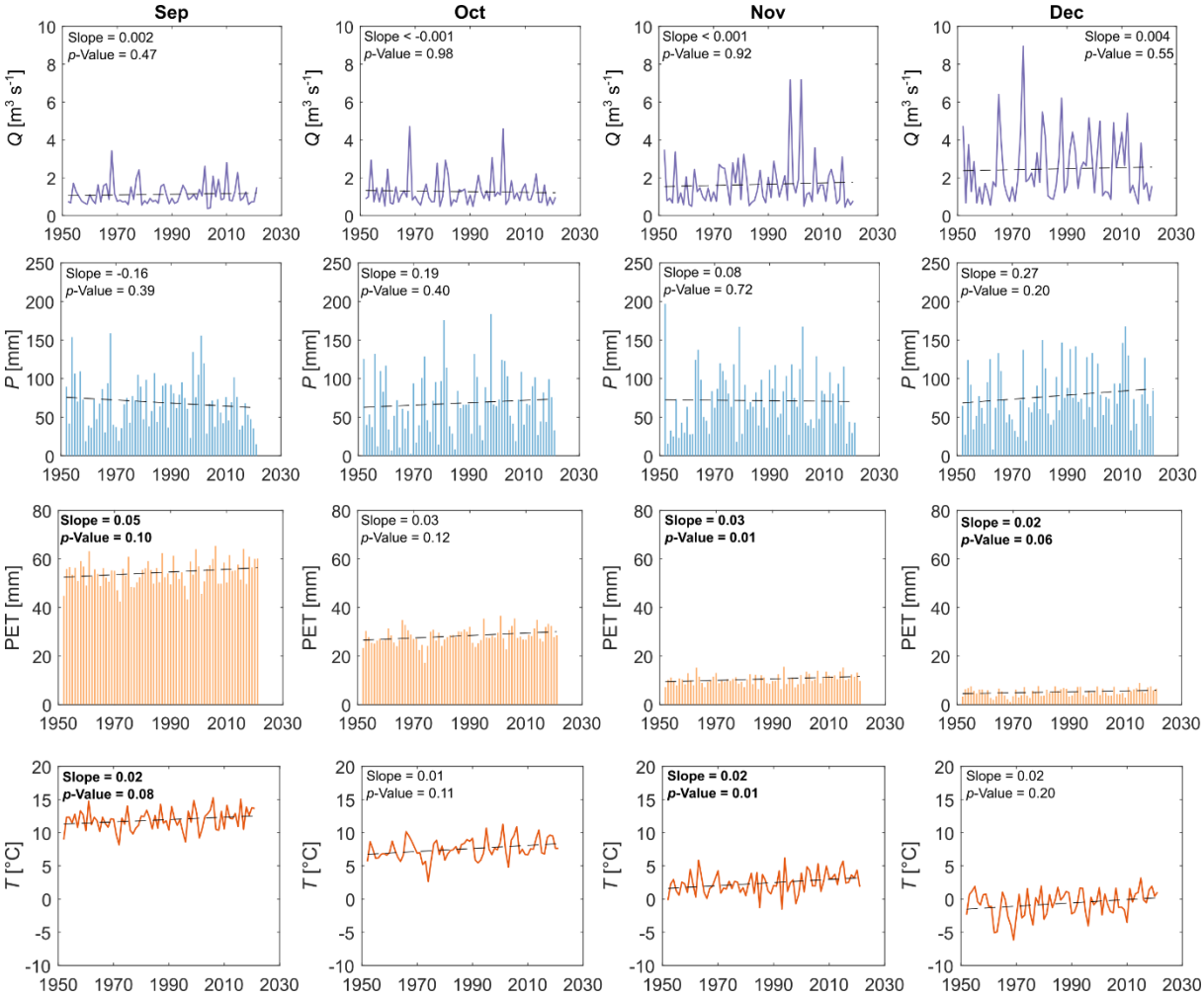

Fig. S4 Trends of the monthly mean discharge (*Q*), total precipitation (*P*), total potential evapotranspiration (PET), and mean temperature (*T*) in September, October, November, and December from 1952 to 2021. The dashed line represents the trend.

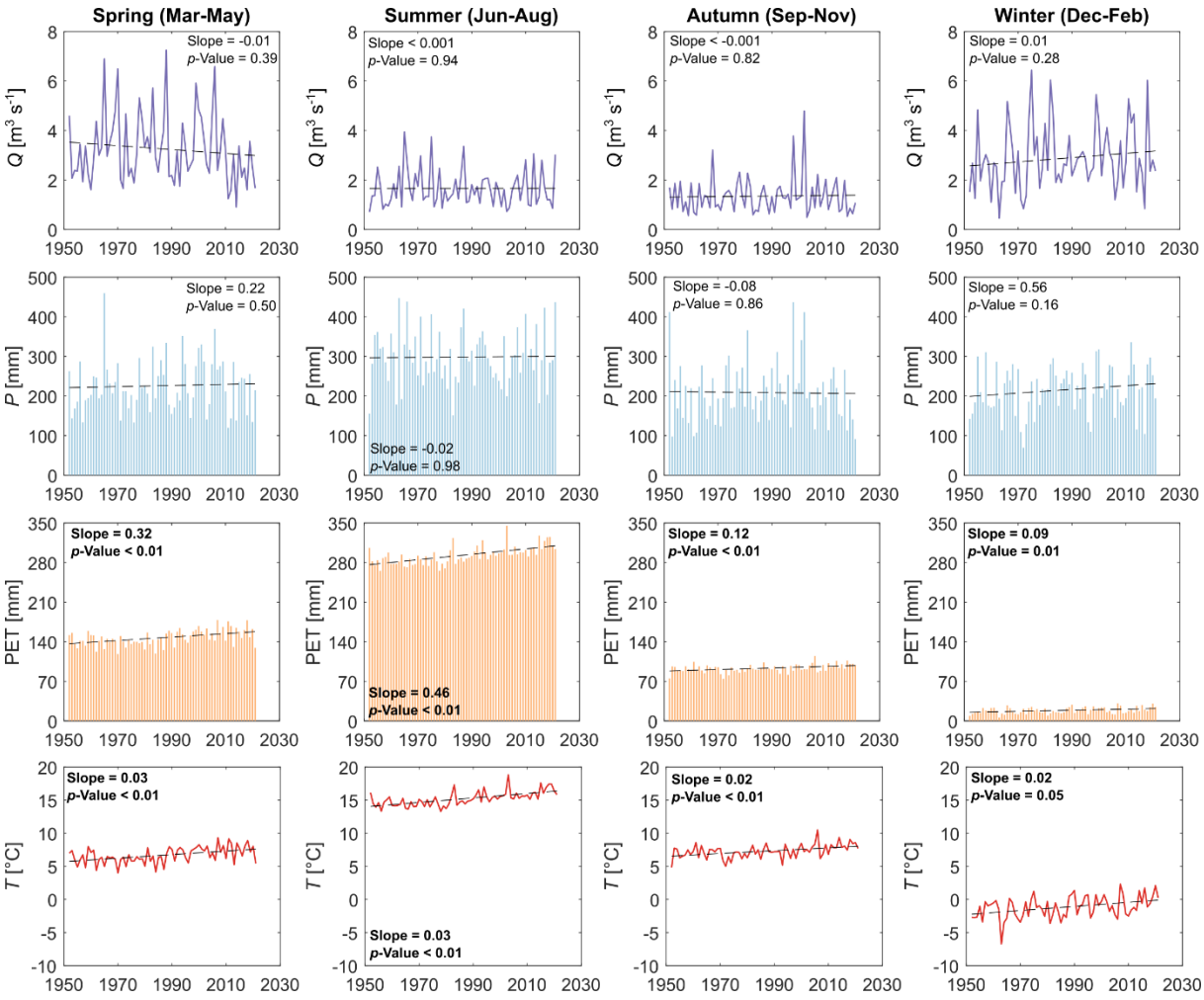

Fig. S5 Trends of the seasonal mean discharge (*Q*), total precipitation (*P*), total potential evapotranspiration (PET), and mean temperature (*T*) in spring (March-May), summer (June-August), autumn (September-November), and winter (December-February) from 1952 to 2020. The dashed line represents the trend.

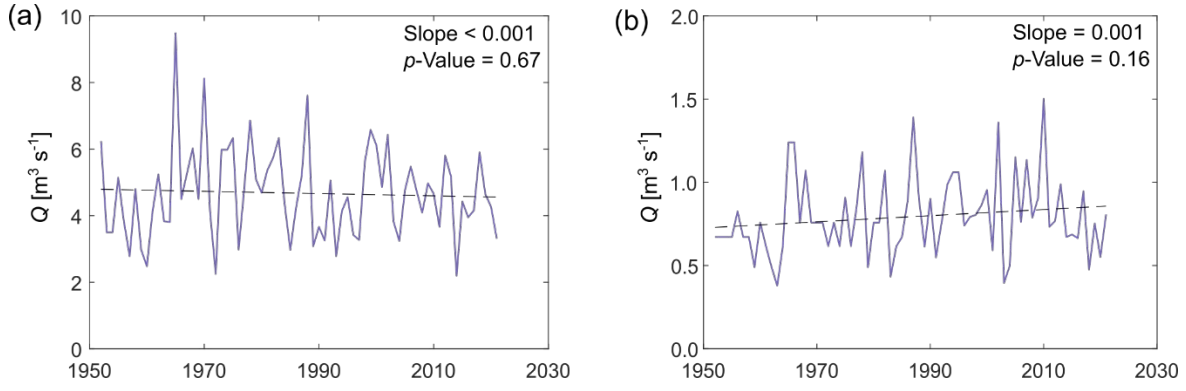

Fig. S6 Trends of the annual mean (a) high discharge (above 90th percentile) and (b) low discharge (below 10th percentile) in the spring from 1952 to 2021. The dashed line represents the trend.

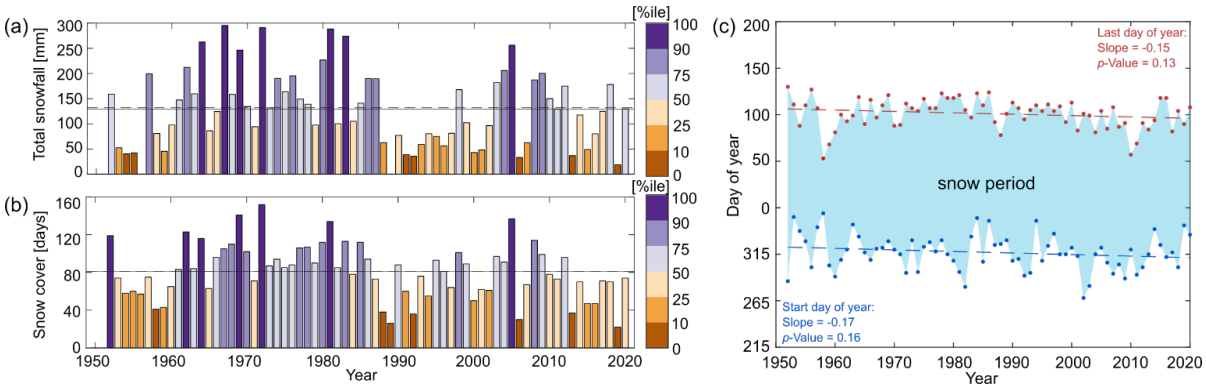

Fig. S7 Annual total snowfall (measured in snow water equivalent) and the length of the snow period (Oct-Apr) at station ID 3402. (a) The annual total snowfall from 1952 to 2020. The records for 1956 and 1989 are lacked. (b) The annual total number of days of the catchment covered in snow. The solid line represents the median and the dashed line represents the mean. The interval of the legend is divided by percentiles (%ile) of the value of the variable. (c) The start day (dark blue dots) and the last day (red dots) of the catchment covered in snow. The light blue block represents the snow period. Note, a one-year cycle is defined from July to June of the next year to cover a continuous snow period.

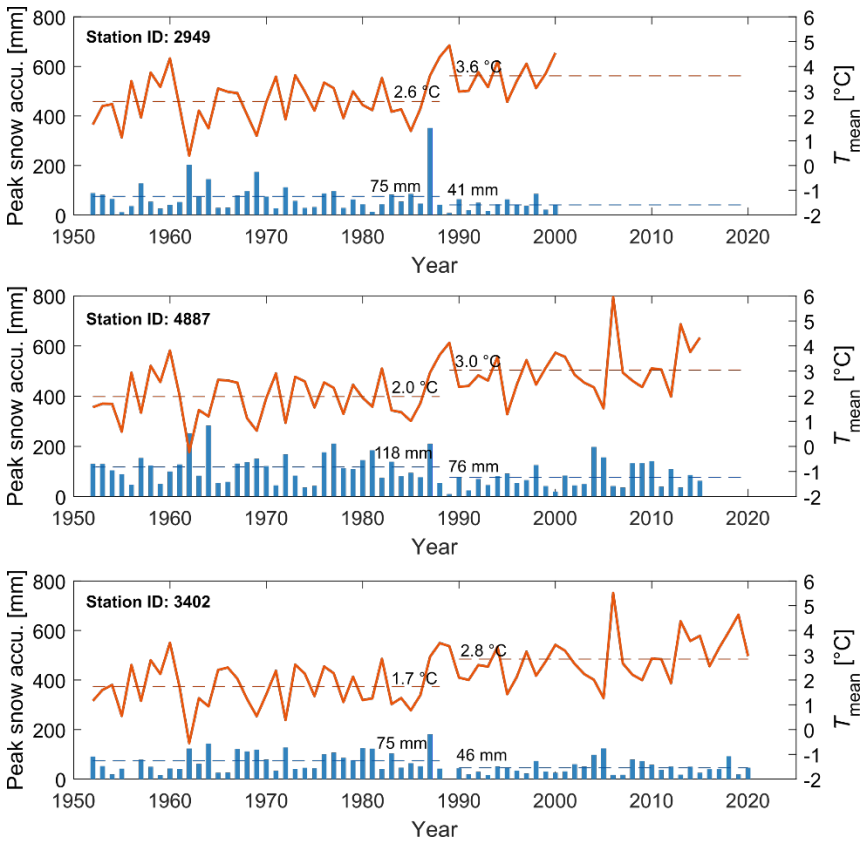

Fig. S8 An abrupt change shown around 1988 in the daily peak snow accumulation (accu., blue bars) and the snow-period (Oct-Apr) mean air temperature (T_{mean}, orange line) at the weather stations (ID: 2949, 4887, and 3402). The numbers are the average calculated before and after the change point. Note, the record in 1989 at station 3402 is lacked.

Table S3 Trends and the most probable change points of the snow-period (Oct-Apr) mean air temperature at the weather stations from 1952 to 2020.

Station ID	Slope [°C yr^{-1}]	*p*-Value	Change point [year]	Probability [%]
2949	0.03	<0.01	1987	34
4887	0.03	<0.01	1987	26
3402	0.03	<0.01	1987	27

Table S4 Trends and the most probable change points of the daily peak snow accumulation at the weather stations from 1952 to 2020.

Station ID	Slope [mm yr^{-1}]	*p*-Value	Change point [year]	Probability [%]
2949	-0.53	0.13	1987	12
4887	-0.82	0.02	1989	17
3402	-0.29	0.13	1988	26

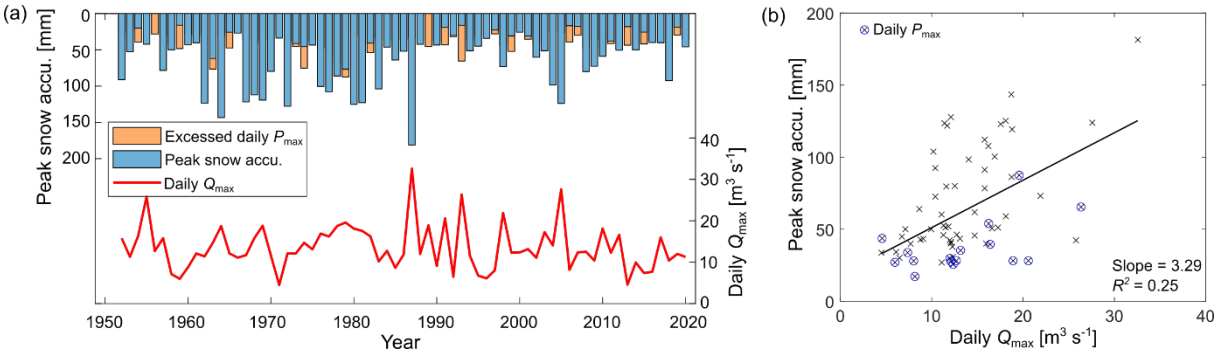

Fig. S9 The peak snow accumulation (accu., measured in snow water equivalent) and the daily discharge maxima (Q_{max}) from 1952 to 2020. The orange bars in (a) represent the excessed amount of the daily precipitation maxima (P_{max}) over the peak snow accumulation. The peak snow accumulation records in 1956 and 1989 are lacked. (b) The daily discharge maxima against the peak snow accumulation. Note, the daily precipitation maxima (blue

circles) are plotted instead when they exceeded the peak snow accumulation. The solid line represents the linear regression that is evaluated with R^2.

S4 Model simulation with *KarstMod*

Table S5 Model parameters, description, and calibrated values. The notation of k_{AB} represents the recession coefficient of the flux from compartment A to B. The E_{min} is fixed as -50 mm.

Parameter	Description	Unit	Parameter ranges		Calibrated value
k_{EM}	Recession coefficient from E to M	d^{-1}	0.10	1.50	0.47
k_{EC}	Recession coefficient from E to C	d^{-1}	0.10	1.50	0.69
k_{MS}	Recession coefficient from M to S	d^{-1}	0.05	0.50	0.18
k_{CS}	Recession coefficient from C to S	d^{-1}	0.005	0.05	0.02
R_A	Recharge area	km^2	150	190	164.70

Table S6 Sobol sensitivity indexes of the calibrated model parameters.

Parameter	First-order index	Total-effect index
k_{MS}	0.18	0.59
k_{EM}	0.14	0.59
k_{EC}	0.07	0.31
R_A	0.03	0.08
k_{CS}	0.01	0.05

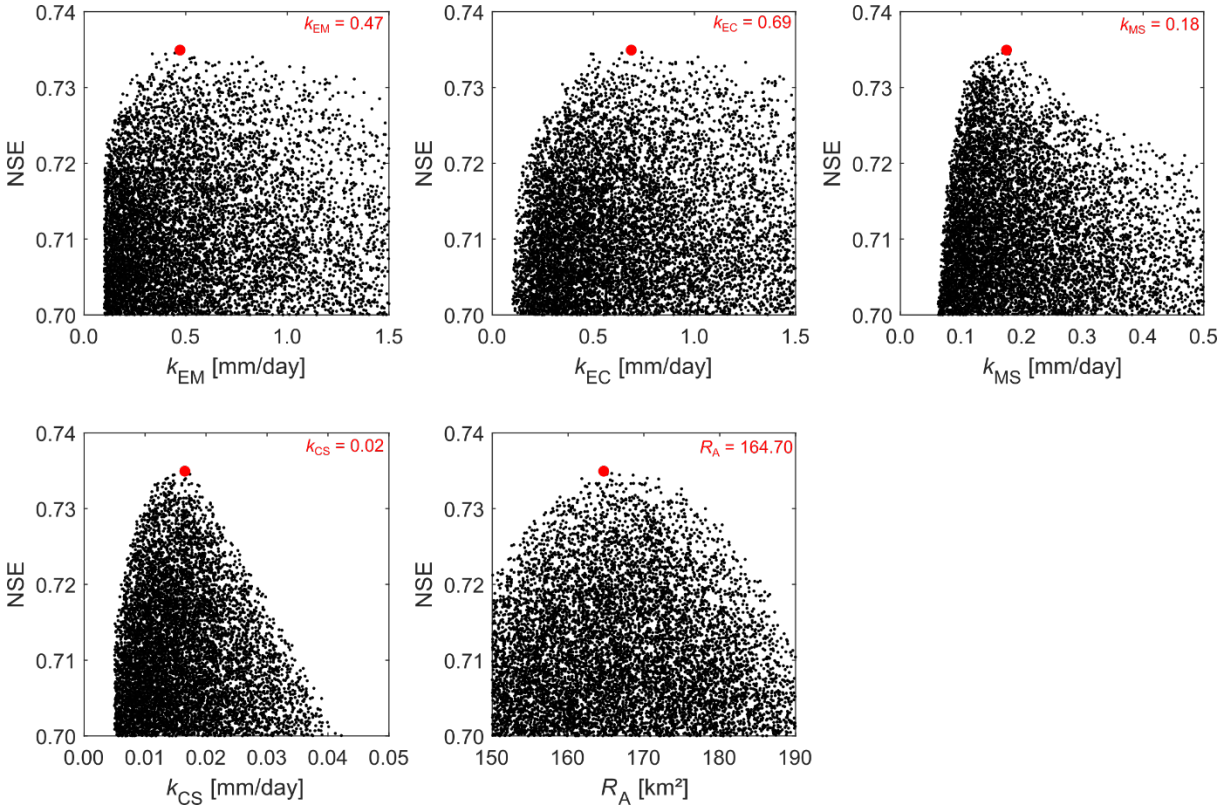

Fig. S10 Sensitivity analysis of the calibrated model parameters with a Monte-Carlo approach. All parameter sets (n=10000) generate an NSE ≥ 0.70. The red dots represent the best parameter set.

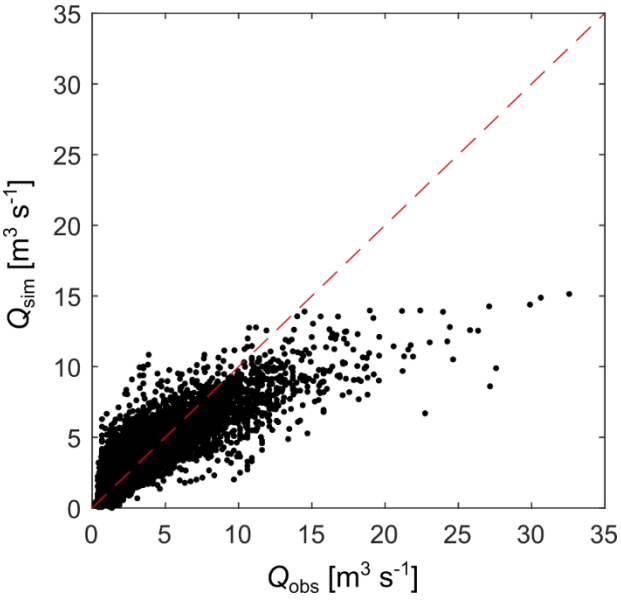

Fig. S11 Comparison between the observed (Q_{obs}) and simulated (Q_{sim}) daily discharge between 1952 and 2021. The red dashed line is a 1:1 reference line.

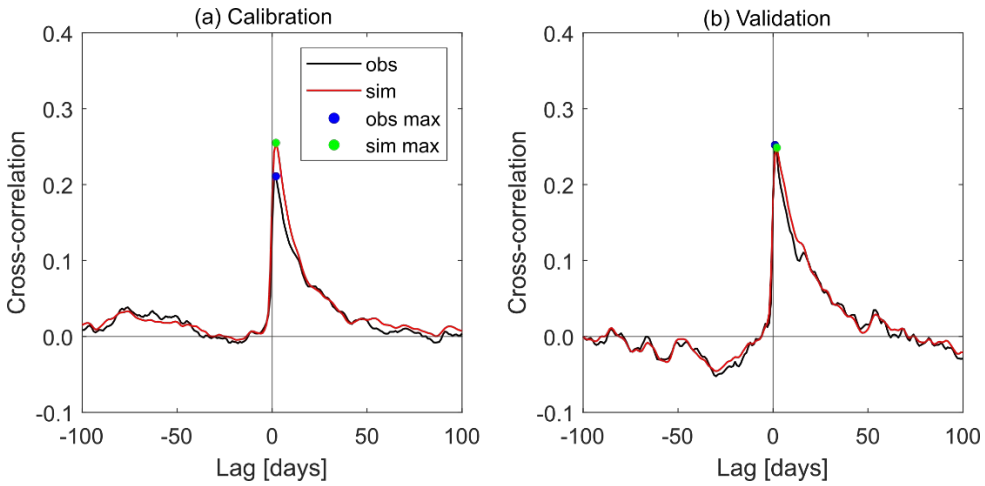

Fig. S12 Cross-correlation functions between the daily discharge and precipitation in the (a) calibration phase and (b) validation phase. The black line represents the observation (obs), the red line represents the simulation (sim), and the blue and green dots represent the lag days at which the observation and simulation achieve their maximum (max) coefficient, respectively.

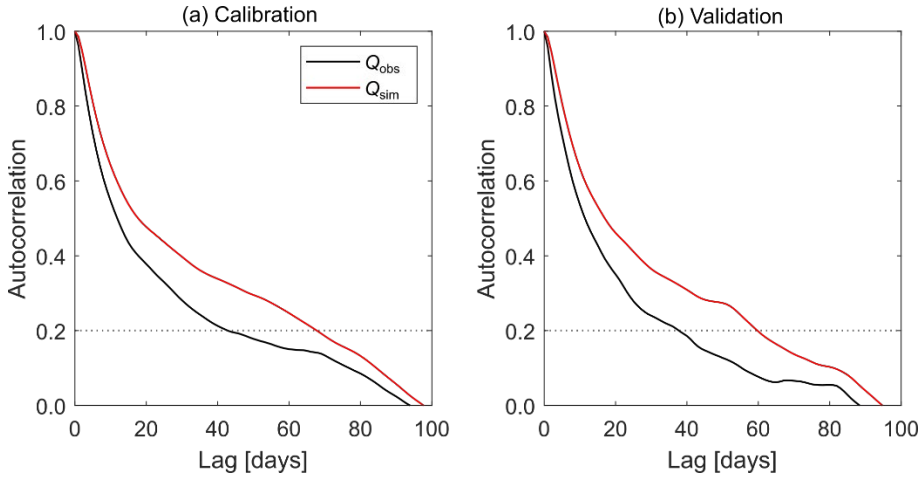

Fig. S13 Autocorrelation functions of the daily observed discharge (Q_{obs}, black line) and simulated discharge (Q_{sim}, red line) in the (a) calibration phase and (b) validation phase.